Characterization of dipping fractures in transversely isotropic background

Vladimir Grechka[⋆] and Ilya Tsvankin[†]

[⋆]Center for Wave Phenomena, Department of Geophysics, Colorado School of Mines, Golden, CO 80401-1887, USA (currently at Shell International Exploration and Production Inc., Bellaire Technology Center, 3737 Bellaire Blvd., Houston, TX 77001-0481, USA)

[†]Center for Wave Phenomena, Department of Geophysics, Colorado School of Mines, Golden, CO 80401-1887, USA

ABSTRACT

Although it is believed that natural fracture sets predominantly have near-vertical orientation, oblique stresses and some other mechanisms may tilt fractures away from the vertical. Here, we examine an effective medium produced by a single system of obliquely dipping rotationally invariant fractures embedded in a VTI (transversely isotropic with a vertical symmetry axis) background rock. This model is monoclinic with a vertical symmetry plane that coincides with the dip plane of the fractures.

Multicomponent seismic data acquired over such a medium possess several distinct features that make it possible to estimate the fracture orientation. For example, the vertically propagating fast shear wave (and the fast converted PS-wave) is typically polarized in the direction of the fracture strike. The normal-moveout (NMO) ellipses of horizontal reflection events are co-oriented with the dip and strike directions of the fractures, which provides an independent estimate of the fracture azimuth. However, the polarization vector of the slow shear wave at vertical incidence does *not* lie in the horizontal plane – an unusual phenomenon that can be used to evaluate fracture dip. Also, for oblique fractures the shear-wave splitting coefficient at vertical incidence becomes dependent on fracture infill (saturation).

A complete medium-characterization procedure includes estimating the fracture compliances and orientation (dip and azimuth), as well as the Thomsen parameters of the VTI background. We demonstrate that both the fracture and background parameters can be obtained from multicomponent wide-azimuth data using the vertical velocities and NMO ellipses of PP-waves and two split SS-waves (or the traveltimes of PS-waves) reflected from horizontal interfaces. Numerical tests corroborate the accuracy and stability of the inversion algorithm based on the exact expressions for the vertical and NMO velocities.

Keywords.—fracture characterization, azimuthal anisotropy, multicomponent seismic, wide-azimuth acquisition, moveout inversion.

INTRODUCTION

Characterization of naturally fractured reservoirs using seismic data is a topic of significant importance to both exploration and reservoir development. Although there exists an extensive list of papers discussing various aspects of fracture detection [many relevant references can be found in the special section of *Geophysics* edited by Tsvankin and Lynn (1999)], very few of them address quantitative inversion of seismic data for fracture parameters. An attempt to fill this gap for several common fracture models was made by Bakulin, Grechka and Tsvankin (2000a,b,c; 2002), who developed fracture-characterization methods based on such reflection seismic signatures as normal-moveout (NMO) ellipses and azimuthally varying AVO (amplitude variation with offset) response of PP- and PS-waves. They showed that while seismic data are generally insufficient to constrain microstructural parameters (the fracture shape, density and the type of infill, equant background porosity, etc.), in many cases they can be used to estimate the orientation and excess compliances of vertical fractures. If additional information about the physical properties of the medium (in particular, about the fluid flow between the fractures and background pores) is available, the compliances can be further inverted for the fracture density and saturation.

While the papers listed above treat vertical fracture sets, there is growing evidence that obliquely dipping fractures are not uncommon. For example, Angerer et al. (2002) identified dipping fractures in the Emilio field (Adriatic Sea) and used the asymmetry of the traveltimes of mode-converted PS-waves to estimate the fracture parameters. Although the combination of fracture dip and background anisotropy (e.g., transverse isotropy) may create rather complicated, low-symmetry anisotropic models, Grechka and Tsvankin (2003) showed that the inversion of seismic data for the fracture compliances and orientations actually becomes better posed if the fractures are rotated away from the vertical.

Here, we generalize the results of Bakulin, Grechka and Tsvankin (2000b), who

studied a set of vertical fractures in a VTI background rock (their model 1), by allowing the fractures to be obliquely dipping. As in our previous work, the linear-slip theory of Schoenberg (1980, 1983) is applied to build a link between the fracture properties and seismic signatures. Note that some deterministic models of penny-shaped cracks/contacts (e.g., Hudson, Liu and Crampin 1996; Liu, Hudson and Pointer 2000) were found to produce an effective medium identical to that of linear slip.

In contrast to the orthorhombic model of Bakulin, Grechka and Tsvankin (2000b), dipping fractures in a VTI background lead to a lower (monoclinic) symmetry of the fractured formation. We study seismic signatures for a wide range of fracture dips and devise a fracture-characterization procedure that uses the vertical velocities and NMO ellipses of reflections from a horizontal interface.

EFFECTIVE MEDIUM AND ANALYSIS OF SEISMIC SIGNATURES

Effective stiffness matrix

Let us consider a set of rotationally invariant dipping fractures with the strike in the x_2-direction embedded in a matrix of VTI symmetry (Figure 1). According to the linear-slip theory (Schoenberg 1980, 1983; Schoenberg and Sayers 1995), the effective compliance matrix $\boldsymbol{s}$ of a fractured medium can be found as the sum of the background compliance $\boldsymbol{s}_b$ and the fracture compliance $\boldsymbol{s}_f$:

$$\boldsymbol{s} = \boldsymbol{s}_b + \boldsymbol{s}_f = \boldsymbol{c}_b^{-1} + \boldsymbol{s}_f \,, \tag{1}$$

where $\boldsymbol{s}$, $\boldsymbol{s}_b$ and $\boldsymbol{s}_f$ are 6×6 symmetric non-negative-definite matrices, and $\boldsymbol{c}_b$ is the stiffness matrix of the VTI background.

The excess compliance matrix $\boldsymbol{s}_f^{x_1}$ of a set of vertical rotationally invariant fractures orthogonal to the x_1-direction can be found in Schoenberg and Sayers (1995) or Bakulin, Grechka and Tsvankin [2000a, equation (6)]. The matrix $\boldsymbol{s}_f^{x_1}$ contains

just two independent elements – the normal fracture compliance K_N and the tangential (shear) compliance K_T. To obtain the compliance matrix for dipping fractures, we apply the so-called Bond transformation to rotate the matrix $\boldsymbol{s}_f^{x_1}$ by the angle θ around the x_2-axis (i.e., around the strike direction):

$$\boldsymbol{s}_f \equiv \boldsymbol{s}_f^{\theta} = \boldsymbol{N}(\theta)\, \boldsymbol{s}_f^{x_1}\, \boldsymbol{N}^T(\theta)\,. \tag{2}$$

$\boldsymbol{N}$ is a 6×6 matrix is explicitly written in Winterstein (1990), and $\boldsymbol{N}^T$ denotes the transposed matrix.

Substituting equation (2) and the well-known expression for the VTI stiffness matrix $\boldsymbol{c}_b$ into equation (1) yields the stiffness matrix of the effective medium in the following form:

$$\boldsymbol{c} \equiv \boldsymbol{s}^{-1} = \begin{pmatrix} c_{11} & c_{12} & c_{13} & 0 & c_{15} & 0 \\ c_{12} & c_{22} & c_{23} & 0 & c_{25} & 0 \\ c_{13} & c_{23} & c_{33} & 0 & c_{35} & 0 \\ 0 & 0 & 0 & c_{44} & 0 & c_{46} \\ c_{15} & c_{25} & c_{35} & 0 & c_{55} & 0 \\ 0 & 0 & 0 & c_{46} & 0 & c_{66} \end{pmatrix}. \tag{3}$$

The matrix $\boldsymbol{c}$ describes a monoclinic medium with a vertical symmetry plane that coincides with the dip plane of the fracture set. This type of symmetry of the effective medium can be predicted from the fact that the dip plane is the only vertical symmetry plane of the fracture set while the VTI background is azimuthally isotropic.

Although the exact expressions for the stiffness coefficients (3) are lengthy, they can be simplified by assuming small background anisotropy and fracture compliances. If the VTI background is weakly anisotropic, the Thomsen (1986) anisotropic coefficients satisfy the inequalities

$$|\,\epsilon_b\,| \ll 1\,, \quad |\,\delta_b\,| \ll 1 \quad \text{and} \quad |\,\gamma_b\,| \ll 1\,. \tag{4}$$

It is convenient to replace the fracture compliances with dimensionless quantities

called the normal (Δ_N) and tangential (Δ_T) weaknesses (Schoenberg and Helbig 1997):

$$\Delta_N \equiv \frac{K_N\, c_{11b}}{1 + K_N\, c_{11b}} \quad \text{and} \quad \Delta_T \equiv \frac{K_T\, c_{44b}}{1 + K_T\, c_{44b}}\,. \tag{5}$$

If the density of fractures is small, the fracture weaknesses are much smaller than unity:

$$\Delta_N \ll 1 \quad \text{and} \quad \Delta_T \ll 1\,. \tag{6}$$

Concise approximations for c_{ij}, obtained by linearizing the exact equations in ϵ_b, δ_b, γ_b, Δ_N and Δ_T, are given in Appendix A. They explicitly show, for example, that the effective medium becomes orthorhombic [this model was examined by Schoenberg and Helbig (1997) and Bakulin, Grechka and Tsvankin (2000b)] when the fractures are vertical (i.e., when the rotation angle $\theta = 0$, which leads to $c_{15} = c_{25} = c_{35} = c_{46} = 0$).

It is important to note that for the fracture azimuth fixed in the x_1-direction, the thirteen elements of the effective stiffness matrix $\boldsymbol{c}$ [equation (3)] depend on just eight independent quantities (two fracture weaknesses, fracture dip and five VTI background parameters). Thus, only eight stiffnesses are independent, and there should be five relationships (constraints) between the elements of $\boldsymbol{c}$. Although those relationships are not apparent even in the limit of weak anisotropy and small fracture weaknesses [equations (A-1)–(A-13)], the fact of their existence is important for identifying the seismic signatures needed for unique fracture characterization.

Phase velocities and polarizations for vertical propagation

Phase velocities and plane-wave polarizations can be determined from the Christoffel matrix G_{ik} (e.g., Helbig 1994; Tsvankin 2001):

$$G_{ik} = c_{ijkl}\, n_j\, n_l - \rho\, V^2\, \delta_{ik}\,, \tag{7}$$

where c_{ijkl} are the components of the stiffness tensor corresponding to the matrix (3), $\boldsymbol{n}$ is a unit vector normal to the wavefront (i.e., $\boldsymbol{n}$ is parallel to the phase-velocity vector), ρ is the density, V is the phase velocity, and δ_{il} is Kronecker's symbolic delta. Summation over repeated indices from 1 to 3 is implied.

Using equation (3) for the effective stiffness tensor, the Christoffel matrix for vertically propagating waves ($\boldsymbol{n} = [0,\, 0,\, 1]$) can be written as

$$\boldsymbol{G} = \begin{pmatrix} c_{55} - \rho\, V^2 & 0 & c_{35} \\ 0 & c_{44} - \rho\, V^2 & 0 \\ c_{35} & 0 & c_{33} - \rho\, V^2 \end{pmatrix}. \tag{8}$$

According to equation (8), one of the vertically traveling S-waves is polarized in the direction [0, 1, 0], which is parallel to the fracture strike. Since the polarization and phase directions for this wave (we denote it $\mathrm{S}_{\parallel}$) are orthogonal, it is a pure shear mode. The phase velocity of the $\mathrm{S}_{\parallel}$-wave is

$$V_{S_{\parallel}} = \sqrt{\frac{c_{44}}{\rho}}\,. \tag{9}$$

Equation (9) and the conclusion about the polarization direction of the $\mathrm{S}_{\parallel}$-wave are valid for any strength of the anisotropy because they are derived from the exact stiffness matrix rather than from the linearized expressions for its elements given in Appendix A.

Using approximation (A-10) for the stiffness c_{44}, the velocity $V_{S_{\parallel}}$ can be expressed through the tangential fracture weakness Δ_T and the deviation angle θ as

$$V_{S_{\parallel}} = V_{S0b}\left(1 - \frac{\Delta_T}{2}\,\sin^2\theta\right), \tag{10}$$

where V_{S0b} is the shear-wave vertical velocity in the VTI background medium.

The phase velocities of the other two vertically propagating waves (P and $\mathrm{S}_{\perp}$) can be found by solving the quadratic equation

$$\det\begin{pmatrix} c_{55} - \rho\, V^2 & c_{35} \\ c_{35} & c_{33} - \rho\, V^2 \end{pmatrix} = 0\,, \tag{11}$$

which follows directly from the Christoffel equation (8). Although both the P- and $S_\perp$-waves are polarized in the $[x_1, x_3]$-plane, the presence of the coefficient c_{35} causes a rotation of their polarization vectors away from the vertical and horizontal directions, respectively. This rotation, which does not exist for vertical fractures, depends on the deviation angle θ and both weaknesses, Δ_N and Δ_T [equation (A-9)]. Hence, the only pure mode (in terms of polarization) traveling in the vertical direction is $S_\parallel$.

It is clear from equation (A-9) for c_{35} that in the linearized weak-anisotropy approximation the term c_{35}^2 in equation (11) can be neglected, and the phase velocities V_P and $V_{S_\perp}$ can be obtained directly from equations (A-8) and (A-12):

$$V_P = \sqrt{\frac{c_{33}}{\rho}} = V_{P0b}\left[1 - \frac{\Delta_N}{2}\left(1 - 2\,g_b + \frac{3\,g_b^2}{2}\right) - \Delta_T\,\frac{g_b}{4} + \Delta_N\,g_b\,(g_b - 1)\,\cos 2\theta + (\Delta_T - g_b\,\Delta_N)\,\frac{g_b}{4}\,\cos 4\theta\right]; \tag{12}$$

$$V_{S_\perp} = \sqrt{\frac{c_{55}}{\rho}} = V_{S0b}\left[1 - \frac{1}{4}\,(g_b\,\Delta_N + \Delta_T) + \frac{1}{4}\,(g_b\,\Delta_N - \Delta_T)\,\cos 4\theta\right]. \tag{13}$$

Here, V_{P0b} is the P-wave vertical velocity in the VTI background medium, and

$$g_b \equiv \frac{V_{S0b}^2}{V_{P0b}^2}. \tag{14}$$

In the special case of vertical fractures ($\theta = 0$), equations (10) and (13) for the velocities $V_{S_\parallel}$ and $V_{S_\perp}$ reduce to the expressions given by Bakulin, Grechka and Tsvankin (2000b):

$$V_{S_\parallel}\Big|_{\theta=0} \equiv V_{S1} = V_{S0b}\,, \tag{15}$$

$$V_{S_\perp}|_{\theta=0} \equiv V_{S2} = V_{S0b}\left(1 - \frac{\Delta_T}{2}\right). \tag{16}$$

Since $0 \le \Delta_T \le 1$, equations (15) and (16) show that the velocity of the S-wave polarized parallel to the fractures is higher than that of the S-wave polarized perpendicular to the fractures (Bakulin, Grechka and Tsvankin 2000b). This fact explains

the notation V_{S1} and V_{S2}, where S_1 and S_2 denote the fast and slow shear waves, respectively:

$$V_{S1} \geq V_{S2}\,. \tag{17}$$

Equations (10) and (13) can be used to determine if the inequality

$$V_{S_\parallel} \geq V_{S_\perp} \tag{18}$$

holds for non-vertical fractures ($\theta \neq 0$). It is clear that inequality (18) is satisfied within a certain range $\theta \geq 0$. To get an estimate of the maximum fracture deviation angle θ for which $V_{S_\parallel} \geq V_{S_\perp}$, we substitute equations (10) and (13) into equation (18) and rewrite it in the form

$$\Delta_T \left(4\,\sin^4\theta - 5\,\sin^2\theta + 1\right) \geq -\,g_b\,\Delta_N\,\sin^2 2\theta\,. \tag{19}$$

The right-hand side of inequality (19) is always non-positive. If the fractures are fluid-filled and $\Delta_N = 0$ (Schoenberg and Sayers 1995), the right-hand side vanishes for all angles θ. The left-hand side of inequality (19) goes to zero for

$$\theta = 30^\circ\,. \tag{20}$$

Hence, for fluid-filled fractures $V_{S_\parallel} \geq V_{S_\perp}$ for the wide range $0^\circ \leq \theta \leq 30^\circ$.

If the fractures are dry, the Schoenberg-Sayers (1995) criterion $K_N = K_T$ yields $\Delta_T \approx g_b\,\Delta_N$ [see equations (5) and (14)]. In this case, any θ from 0° to 90° satisfies inequality (19), and $V_{S_\parallel} \geq V_{S_\perp}$ for the whole range of fracture dips.

Since the above comparisons between the shear-wave vertical velocities are based on the assumption of weak background anisotropy and small fracture weaknesses, it is useful to verify them using the exact equations. The shear-wave velocities in Fig. 2 are computed for a moderately anisotropic VTI background and a substantial value of the crack density $e \approx \Delta_T/2 = 0.1$. Evidently, approximation (20) for fluid-filled fractures is quite accurate, and $V_{S_\parallel} > V_{S_\perp}$ until the angle θ reaches a value close to 30°

(Fig. 2a). However, the weak-anisotropy prediction that for dry fractures $V_{S_\parallel} > V_{S_\perp}$ does not hold for near-horizontal fracture orientation (Fig. 2b).

Comparison of Figs. 2a and 2b proves that, in agreement with approximation (10), the exact velocity $V_{S_\parallel}$ depends just on the tangential weakness and is insensitive to the fracture infill. In contrast, for obliquely dipping fractures the velocity of the wave $S_\perp$ [equation (13)] and the splitting coefficient at vertical incidence also depend on the normal compliance Δ_N that varies with fluid saturation (Figure 2). Note that the exact splitting coefficient for oblique fractures should be computed from the vertical group velocities, which are somewhat different from the corresponding phase velocities.

NMO velocities from a horizontal reflector

To estimate the VTI background parameters and fracture weaknesses, the velocities and polarization directions of the vertically propagating waves can be supplemented by the NMO velocities of P- and S-waves from a horizontal interface. The NMO velocity of any pure (non-converted) reflection mode can be expressed as the following function of the azimuth α (Grechka and Tsvankin 1998; Tsvankin 2001):

$$V_{\rm nmo}^{-2}(\alpha) = W_{11}\cos^2\alpha + 2\,W_{12}\sin\alpha\cos\alpha + W_{22}\sin^2\alpha\,. \qquad (21)$$

The elements of the 2×2 symmetric matrix $\boldsymbol{W}$ can be expressed through the derivatives of the horizontal components p_1 and p_2 of the slowness vector with respect to the source or receiver coordinates. If reflection traveltime in common-midpoint (CMP) geometry increases with offset for all azimuthal directions (the usual case), the eigenvalues of $\boldsymbol{W}$ are positive, and equation (21) describes an ellipse.

For a homogeneous medium above the reflector, the matrix $\boldsymbol{W}$ takes the form (Grechka, Tsvankin and Cohen 1999)

$$\boldsymbol{W} = \frac{p_1 q_{,1} + p_2 q_{,2} - q}{q_{,11} q_{,22} - q_{,12}^2} \begin{pmatrix} q_{,22} & -q_{,12} \\ -q_{,12} & q_{,11} \end{pmatrix}, \tag{22}$$

where $q(p_1, p_2)$ is the vertical slowness, $q_{,i} \equiv \partial q / \partial p_i$ and $q_{,ij} \equiv \partial^2 q / \partial p_i \partial p_j$. The slowness components and their derivatives in equation (22) are evaluated for the zero-offset ray.

If the reflector is horizontal, the zero-offset slowness vector is vertical ($p_1 = p_2 = 0$) and equation (22) reduces to

$$\boldsymbol{W} = \frac{-q}{q_{,11} q_{,22} - q_{,12}^2} \begin{pmatrix} q_{,22} & -q_{,12} \\ -q_{,12} & q_{,11} \end{pmatrix}. \tag{23}$$

For the effective monoclinic medium treated here, the dip plane of the fractures represents a vertical symmetry plane of the model. (Note that there is only one symmetry plane in monoclinic media.) Therefore, the axes of all three pure-mode NMO ellipses should be parallel to the dip and strike directions of the fracture set (Grechka and Tsvankin 1998). Indeed, since the x_1-axis is aligned with the fracture dip and the vertical symmetry plane, the derivative $q_{,12}$ vanishes, and the matrix (23) becomes diagonal:

$$\boldsymbol{W} = \begin{pmatrix} -q/q_{,11} & 0 \\ 0 & -q/q_{,22} \end{pmatrix}. \tag{24}$$

From equation (24) it follows that the NMO velocities in the dip and strike directions are given by

$$V_{\rm nmo}^{\rm dip} = \sqrt{\frac{-q_{,11}}{q}} \quad \text{and} \quad V_{\rm nmo}^{\rm str} = \sqrt{\frac{-q_{,22}}{q}}\,. \tag{25}$$

Next, we assume weak background anisotropy and small fracture weaknesses [equations (4) and (6)] and derive linearized expressions for $V_{\rm nmo}^{\rm dip}$ and $V_{\rm nmo}^{\rm str}$ similar to those obtained above for the phase velocities.

$$V_{{\rm nmo},P}^{\rm dip} = V_{P0b} \left[1 + \delta_b + \Delta_N \left(g_b - \frac{1}{2} - \frac{3\, g_b^2}{4} \right) - \frac{g_b}{4}\, \Delta_T \right.$$

$$-\Delta_N\, g_b\,(1-g_b)\,\cos 2\theta - \frac{7\,g_b}{4}\,(\Delta_T - g_b\,\Delta_N)\,\cos 4\theta\Bigg], \tag{26}$$

$$V^{\rm str}_{{\rm nmo},P} = V_{P0b}\Bigg[1+\delta_b+\Delta_N\left(2\,g_b-\frac{1}{2}-\frac{5\,g_b^2}{4}\right)-\frac{3\,g_b}{4}\,\Delta_T + g_b\,(\Delta_T - g_b\,\Delta_N)\,\cos 2\theta - \frac{g_b}{4}\,(\Delta_T - g_b\,\Delta_N)\,\cos 4\theta\Bigg], \tag{27}$$

$$V^{\rm dip}_{{\rm nmo},S_\parallel} = V_{S0b}\left(1+\gamma_b+\frac{\Delta_T}{2}\,\cos^2\theta\right), \tag{28}$$

$$V^{\rm str}_{{\rm nmo},S_\parallel} = V_{S0b}\left(1+\frac{\epsilon_b-\delta_b}{g_b}\right), \tag{29}$$

$$V^{\rm dip}_{{\rm nmo},S_\perp} = V_{S0b}\left[1+\frac{\epsilon_b-\delta_b}{g_b}-\frac{1}{4}\,(\Delta_T+g_b\,\Delta_N)+\frac{7}{4}\,(\Delta_T-g_b\,\Delta_N)\,\cos 4\theta\right], \tag{30}$$

$$V^{\rm str}_{{\rm nmo},S_\perp} = V_{S0b}\Bigg[1+\gamma_b+\frac{1}{4}\,(\Delta_T-3\,g_b\,\Delta_N) -(\Delta_T-g_b\,\Delta_N)\,\cos 2\theta+\frac{1}{4}\,(\Delta_T-g_b\,\Delta_N)\,\cos 4\theta\Bigg]. \tag{31}$$

Equations (26) and (27) show that in the linear approximation the azimuthal variation of the P-wave NMO velocity is independent of the background anisotropic coefficients. Also, it is possible to combine the dip and strike components of the shear-wave NMO ellipses [equations (28)–(31)] in such a way that the result depends just on the fracture parameters and the background vertical velocities. Next, we introduce the anisotropic coefficients $\chi_{_P}$, $\tilde{\chi}_{_S}$ and $\hat{\chi}_{_S}$ responsible for the influence of azimuthal anisotropy on the NMO ellipses.

$$\chi_{_P} \equiv V^{\rm dip}_{P,\,{\rm nmo}} - V^{\rm str}_{P,\,{\rm nmo}}$$

$$= 2\,g_b\,V_{P0b}\,\cos^2\theta\,[\,2\,\Delta_T - \Delta_N\,(1+g_b) - 3\,(\Delta_T - g_b\,\Delta_N)\,\cos 2\theta\,], \tag{32}$$

$$\tilde{\chi}_S \equiv V^{\rm dip}_{S_\parallel,\,\rm nmo} - V^{\rm str}_{S_\perp,\,\rm nmo} = V_{S0b}\,\sin^2\theta\left[\,g_b\,\Delta_N - \frac{\Delta_T}{2} + (\Delta_T - g_b\,\Delta_N)\,\cos 2\theta\,\right], \qquad (33)$$

$$\hat{\chi}_S \equiv V^{\rm dip}_{S_\perp,\,\rm nmo} - V^{\rm str}_{S_\parallel,\,\rm nmo} = V_{S0b}\,\left[\,-\Delta_T - g_b\,\Delta_N + 7\,(\Delta_T - g_b\,\Delta_N)\,\cos 4\theta\,\right]. \qquad (34)$$

The structure of equations (32)–(34) is a direct consequence of the "addition rule" for the background and fracture-related anisotropic coefficients described by Bakulin, Grechka and Tsvankin (2000b). Since the NMO ellipses of pure-mode horizontal events degenerate into circles in VTI media, the contribution of the background anisotropy can be eliminated by subtracting the NMO velocities measured at different azimuths.

According to equation (32), the semi-major axis of the P-wave NMO ellipse points in the strike direction if the fractures do not strongly deviate from the vertical. Indeed, χ_P is always negative for dry fractures ($\Delta_T \approx g_b\,\Delta_N$), while for fluid-filled fractures ($\Delta_N = 0$) $\chi_P < 0$ if $\theta < 24^\circ$. Thus, the azimuth of the semi-major axis of the P-wave NMO ellipse can be used (in addition to the fast shear-wave polarization at vertical incidence) to estimate the strike azimuth.

The vertical velocities [equations (10), (12), (13)] and the NMO coefficients χ_P, $\tilde{\chi}_S$ and $\hat{\chi}_S$ [equations (32)–(34)] yield six equations which contain five unknowns: the weaknesses Δ_N and Δ_T, the fracture deviation angle θ, and the background velocities V_{P0b} and V_{S0b}. It is possible to prove that all five parameters can be resolved individually from the linearized equations. The background anisotropic coefficients ϵ_b, δ_b and γ_b can then be obtained from the semi-axes of the NMO ellipses of P-waves and one of the S-waves. Below we study the stability of parameter estimation using the *exact* expressions for the vertical velocities and NMO ellipses.

FRACTURE CHARACTERIZATION

Here, we discuss the inversion of seismic data for the fracture and background parameters of a horizontal fractured layer. The fast and slow shear waves at small and moderate incidence angles can be separated, both in vertical seismic profiling (VSP) and reflection surveys, using Alford (1986) rotation. If the vertical component of the polarization vector of the slow S-wave at near-vertical incidence cannot be neglected, the rotation has to be performed in three dimensions (i.e., using all three displacement components). As demonstrated above, the polarization vector of the fast shear wave at vertical incidence points in the direction of the fracture strike, while the deviation of the slow S-wave polarization from the horizontal plane serves as an indicator of obliquely dipping fractures.

If shear waves are not excited, they can be replaced in polarization analysis by mode-converted (PS) waves using the algorithms described by Thomsen (1988) and Thomsen, Tsvankin and Mueller (1999). The shear-wave traveltimes and, therefore, NMO ellipses can also be obtained from mode conversions using 3-D multi-azimuth PP and PS (PS_1 and PS_2) reflection data. This can be accomplished by applying the methodology of Grechka and Tsvankin (2002) designed to reconstruct the traveltimes of the pure SS-waves from PP and PS data prior to anisotropic velocity analysis.

Note that the absence of a horizontal symmetry plane makes converted-wave reflection traveltimes asymmetric with respect to zero offset; such asymmetry is usually observed for dipping reflectors (e.g., Tsvankin and Grechka 2000). Fig. 3 displays a typical traveltime curve of the $PS_\perp$-wave (or PS_2-wave) calculated along a line in the dip direction of dry fractures. Since for this line the $PS_\perp$-wave is polarized within the incidence plane, it is a PSV-type mode. Although the reflector is horizontal, the moveout in Fig. 3 is asymmetric with respect to zero offset because interchanging the source and receiver yields a different converted-wave traveltime. This moveout asymmetry of mode conversions was used by Angerer et al. (2002) to characterize

dipping fractures. The algorithm of Grechka and Tsvankin (2002) generates the pure SS-wave traveltimes, which are symmetric (i.e., reciprocal with respect to the source and receiver positions) in common-midpoint geometry but still contain information about the dip of the fracture set.

The pure-mode NMO ellipses (Fig. 4) can then be reconstructed by means of 3-D (azimuthal) velocity analysis of the PP and SS data (Grechka and Tsvankin 1999). After building the "effective" NMO ellipses for the reflections from the top and bottom of the fractured layer, one can compute the interval NMO ellipses using the generalized Dix equation (Grechka, Tsvankin and Cohen 1999). To constrain both the fracture and background parameters for the model at hand, the NMO ellipses of the PP-wave and two split SS-waves have to be supplemented with their vertical velocities, which are assumed to be measured in a borehole.

The results in Fig. 5 are obtained for a set of dry fractures by applying nonlinear inversion based on the exact equations for the vertical velocities and NMO ellipses of all three pure modes. To verify the stability of the inversion algorithm, we added Gaussian noise with the standard deviations of 0.5% and 2% to the vertical and NMO velocities, respectively. The inversion was repeated 100 times for different realizations of the noise to find the standard deviation of each parameter. The confidence intervals for the background anisotropic coefficients and the tangential weakness Δ_T are close to 0.02, which indicates that the inversion is sufficiently stable.

For the normal weakness Δ_N, however, the confidence interval is much more broad (it reaches 0.06). The reason for the lower accuracy in estimating Δ_N can be explained by the weak-anisotropy approximations discussed in the previous section. Equations (10), (12), (13) and (26)–(31) show that most terms containing the weakness Δ_N have the multiplier g_b, which is relatively small (close to 0.2 in our model). As a result, the sensitivity of the velocities to Δ_N is lower compared to that with respect to other anisotropic parameters, and the errors in Δ_N are greater.

Similar inversion results with somewhat smaller error bars were obtained for fluid-

filled fractures (Fig. 6). Note that the confidence interval for the normal weakness Δ_N includes a range of negative values, although Δ_N is supposed to be positive. The inversion produces those nonphysical values of Δ_N when random errors added to the data lead to velocities that do not correspond to any effective fractured medium.

DISCUSSION AND CONCLUSIONS

Literature on seismic fracture detection is largely devoted to characterization of vertical fracture sets. Seismic data were proved to be sufficient for estimating the orientations and compliances of vertical fractures for several typical effective anisotropic models with symmetries ranging from HTI to monoclinic to triclinic (Bakulin, Grechka and Tsvankin 2000a,b,c, 2002; Grechka, Bakulin and Tsvankin 2003). Subsurface fractures, however, may be rotated away from the vertical by strong oblique stresses and other factors (Angerer et al. 2002). Here, we discussed the parameter-estimation problem for an obliquely dipping set of rotationally invariant fractures embedded in a VTI background rock. Such a medium is monoclinic and has a vertical symmetry plane parallel to the dip direction of the fractures.

Seismic signatures for this model have some similarities with those for the higher-symmetry (orthorhombic and HTI) media produced by vertical fractures in a VTI or isotropic background (Bakulin, Grechka and Tsvankin 2000a,b). In particular, if the fractures do not deviate far from the vertical (up to 25–30°), both the polarization vector of the vertically propagating fast S-wave and the semi-major axis of the P-wave NMO ellipse for horizontal reflectors point in the direction of the fracture strike.

However, for obliquely dipping fractures the vertically traveling P-wave and slow S-wave are *not* polarized in the vertical direction and horizontal plane, respectively. Their polarization vectors are rotated within the dip plane of the fractures around the fracture strike by an angle dependent on the fracture dip and weaknesses. Therefore, a substantial vertical displacement component of the slow S-wave (or a horizontal

component of the P-wave) at near-vertical incidence serves as a strong indicator of oblique fractures. Also, as the fractures deviate from the vertical, the velocity of the slow S-wave and the shear-wave splitting coefficient at vertical incidence become sensitive to fracture infill (i.e., to fluid saturation).

Although the effective medium is monoclinic, it is described by just nine (rather than 13) independent quantities: the VTI background parameters V_{P0b}, V_{S0b}, ϵ_b, δ_b, and γ_b, the normal and tangential fracture weaknesses Δ_N and Δ_T, the fracture azimuth, and the fracture deviation angle θ. This reduction in the number of independent medium parameters facilitates fracture characterization and evaluation of the background anisotropy using seismic data. We showed that all independent parameters listed above can be estimated from the vertical velocities of P-waves and two split S-waves and their NMO ellipses for horizontal reflectors. The method of Grechka and Tsvankin (2002) can be applied prior to the anisotropic inversion to replace the pure shear modes in the fracture-characterization procedure by the split converted (PS) waves.

The feasibility of the parameter estimation was demonstrated using the weak-anisotropy approximation and confirmed by numerical inversion of noise-contaminated data based on the exact equations. Although the normal weakness Δ_N is estimated with a somewhat lower accuracy than the rest of the anisotropic parameters, but the overall performance of the inversion algorithm is quite satisfactory.

The model treated here includes a single set of fractures, but the results of Grechka and Tsvankin (2003) indicate that it may be possible to invert seismic data for the parameters of up to *four* dipping, rotationally invariant fracture sets in a VTI background.

ACKNOWLEDGEMENTS

We are grateful to members of the A(nisotropy)-Team of the Center for Wave Phenomena (CWP), Colorado School of Mines, for helpful discussions and to Ken Larner and Andres Pech for reviewing the manuscript. Suggestions of the editor (E. Liu) and reviewers of *Geophysical Prospecting* helped to improve the text. The support for this work was provided by the sponsors of the Consortium Project on Seismic Inverse Methods for Complex Structures at CWP and by the Chemical Sciences, Geosciences and Biosciences Division, Office of Basic Energy Sciences, U.S. Department of Energy.

REFERENCES

Alford R.M. 1986. Shear data in the presence of azimuthal anisotropy. 56th SEG meeting, Houston, USA, Expanded Abstracts, 476–479.

Angerer E., Horne S. A., Gaiser J. E., Walters R., Bagala S. and Vetri L. 2002. Characterization of dipping fractures using PS mode-converted data. 72nd SEG meeting, Salt Lake City, USA, Expanded Abstracts, 1010–1013.

Bakulin A., Grechka V. and Tsvankin I. 2000a. Estimation of fracture parameters from reflection seismic data – Part I: HTI model due to a single fracture set. *Geophysics* **65**, 1788–1802.

Bakulin A., Grechka V. and Tsvankin I. 2000b. Estimation of fracture parameters from reflection seismic data – Part II: Fractured models with orthorhombic symmetry. *Geophysics* **65**, 1803–1817.

Bakulin A., Grechka V. and Tsvankin I. 2000c. Estimation of fracture parameters from reflection seismic data – Part III: Fractured models with monoclinic symmetry. *Geophysics* **65**, 1818–1830.

Bakulin A., Grechka V. and Tsvankin I. 2002. Seismic inversion for the parameters of two orthogonal fracture sets in a VTI background medium. *Geophysics* **67**, 289–296.

Grechka V., Bakulin A. and Tsvankin I. 2003. Seismic characterization of vertical fractures described as general linear-slip interfaces. *Geophysical Prospecting* **51**, 117–130.

Grechka V. and Tsvankin I. 1998. 3-D description of normal moveout in anisotropic inhomogeneous media. *Geophysics* **63**, 1079–1092.

Grechka V. and Tsvankin I. 1999. 3-D moveout inversion in azimuthally anisotropic media with lateral velocity variation: Theory and a case study. *Geophysics* **64**, 1202–1218.

Grechka V. and Tsvankin I. 2002. PP + PS = SS. *Geophysics* **67**, 1961–1971.

Grechka V. and Tsvankin I. 2003. Feasibility of seismic characterization of multiple fracture sets: *Geophysics* **68**, 1399–1407.

Grechka V., Tsvankin I. and Cohen J.K. 1999. Generalized Dix equation and analytic treatment of normal-moveout velocity for anisotropic media. *Geophysical Prospecting* **47**, 117–148.

Helbig K. 1994. *Foundations of elastic anisotropy for exploration seismics*. Pergamon Press.

Hudson J.A., Liu E. and Crampin S. 1996. Transmission properties of a plane fault. *Geophysical Journal International* **125**, 559–566.

Liu E., Hudson J.A. and Pointer T. 2000. Equivalent medium representation of fractured rock. *Journal of Geophysical Research* **105**, No. B2, 2981–3000.

Schoenberg M. 1980. Elastic wave behavior across linear slip interfaces. *Journal of the Acoustical Society of America* **68**, 1516–1521.

Schoenberg M. 1983. Reflection of elastic waves from periodically stratified media with interfacial slip. *Geophysical Prospecting* **31**, 265–292.

Schoenberg M. and Helbig K. 1997. Orthorhombic media: Modeling elastic wave behavior in a vertically fractured earth. *Geophysics* **62**, 1954–1974.

Schoenberg M. and Sayers C. 1995. Seismic anisotropy of fractured rock. *Geophysics* **60**, 204–211.

Thomsen L. 1986. Weak elastic anisotropy. *Geophysics* **51**, 1954–1966.

Thomsen L. 1988. Reflection seismology over azimuthally anisotropic media. *Geophysics* **53**, 304–313.

Thomsen L., Tsvankin I. and Mueller M.C. 1999. Coarse-layer stripping of vertically variable azimuthal anisotropy from shear-wave data. *Geophysics* **64**, 1126–1138.

Tsvankin I. 2001. *Seismic signatures and analysis of reflection data in anisotropic media*. Elsevier Science Publishing Co.

Tsvankin I. and Grechka V. 2000. Dip moveout of converted waves and parameter estimation in transversely isotropic media. *Geophysical Prospecting* **48**, 257–292.

Tsvankin I. and Lynn H.B. 1999. Special section on azimuthal dependence of P-wave seismic signatures – Introduction. *Geophysics* **64**, 1139–1142.

Winterstein D.F. 1990. Velocity anisotropy terminology for geophysicists. *Geophysics* **55**, 1070–1088.

APPENDIX A–WEAK-ANISOTROPY APPROXIMATION FOR THE EFFECTIVE STIFFNESS COEFFICIENTS

Here we give simplified expressions for the elements of the effective stiffness matrix (3) derived for models with weak background anisotropy [equation (4)] and small fracture weaknesses [equation (6)]. Assuming that the background anisotropic coefficients and fracture weaknesses are of the same order, equations (1) and (2) can be linearized in those quantities to obtain the following approximate stiffness coefficients (3):

$$c_{11} = \rho\, V_{P0b}^2 \left[1 + 2\,\epsilon_b - \Delta_N \left(1 - 2\,g_b + \frac{3\,g_b^2}{2} \right) - \frac{g_b}{2}\,\Delta_T \right.$$
$$\left. + 2\,\Delta_N\, g_b\,(1 - g_b)\,\cos 2\theta + \frac{g_b}{2}\,(\Delta_T - g_b\,\Delta_N)\,\cos 4\theta \right], \tag{A-1}$$

$$c_{12} = \rho\, V_{P0b}^2 \left[1 - 2\,g_b + 2\,\epsilon_b - 4\,g_b\,\gamma_b - \Delta_N \left(1 - 3\,g_b + 2\,g_b^2 \right) \right.$$
$$\left. + \Delta_N\, g_b\,(2\,g_b - 1)\,\cos 2\theta \right], \tag{A-2}$$

$$c_{13} = \rho\, V_{P0b}^2 \left[1 - 2\,g_b + \delta_b - \Delta_N \left(1 - 2\,g_b + \frac{g_b^2}{2} \right) + \frac{g_b}{2}\,\Delta_T \right.$$
$$\left. + \frac{g_b}{2}\,(g_b\,\Delta_N - \Delta_T)\,\cos 4\theta \right], \tag{A-3}$$

$$c_{15} = \rho\, V_{S0b}^2\, \left[\Delta_N\,(1 - g_b) + (g_b\,\Delta_N - \Delta_T)\,\cos 2\theta \right] \sin 2\theta, \tag{A-4}$$

$$c_{22} = \rho\, V_{P0b}^2\, \left[1 + 2\,\epsilon_b - \Delta_N\,(1 - 2\,g_b)^2 \right], \tag{A-5}$$

$$c_{23} = \rho\, V_{P0b}^2\, \left[1 - 2\,g_b + \delta_b - \Delta_N\,(1 - 2\,g_b)\,(1 - g_b) + \Delta_N\, g_b\,(1 - 2\,g_b)\,\cos 2\theta \right], \tag{A-6}$$

$$c_{25} = \rho\, V_{S0b}^2\, \Delta_N\,(1 - 2\,g_b)\,\sin 2\theta, \tag{A-7}$$

$$c_{33} = \rho\, V_{P0b}^2 \left[1 - \Delta_N \left(1 - 2\, g_b + \frac{3\, g_b^2}{2} \right) - \frac{g_b}{2}\, \Delta_T \right.$$
$$\left. + 2\, \Delta_N\, g_b\, (g_b - 1)\, \cos 2\theta + \frac{g_b}{2}\, (\Delta_T - g_b\, \Delta_N)\, \cos 4\theta \right], \tag{A-8}$$

$$c_{35} = \rho\, V_{S0b}^2\, \left[\Delta_N\, (g_b - 1) + (\Delta_T - g_b\, \Delta_N)\, \cos 2\theta \right] \sin 2\theta, \tag{A-9}$$

$$c_{44} = \rho\, V_{S0b}^2 \left(1 - \Delta_T\, \sin^2 \theta \right), \tag{A-10}$$

$$c_{46} = \rho\, V_{S0b}^2\, \Delta_T\, \sin\theta\, \cos\theta\,, \tag{A-11}$$

$$c_{55} = \rho\, V_{S0b}^2 \left[1 - \frac{1}{2}\, (g_b\, \Delta_N + \Delta_T) + \frac{1}{2}\, (g_b\, \Delta_N - \Delta_T)\, \cos 4\theta \right], \tag{A-12}$$

$$c_{66} = \rho\, V_{S0b}^2 \left(1 + 2\, \gamma_b - \Delta_T\, \cos^2 \theta \right). \tag{A-13}$$

The elements of the stiffness matrix c_{ij} not listed here are equal to zero. All quantities used in equations (A-1)–(A-13) are defined in the main text.

FIGURES

FIG. 1. Orientation of a fracture set is described by the dip θ and azimuth ϕ of the vector $\boldsymbol{n}$ orthogonal to the fracture plane. Since the background is azimuthally isotropic, we assume that the fracture strike is parallel to the x_2-axis, and $\phi = 0$.

FIG. 2. Exact vertical phase velocities of the shear waves polarized in the dip plane (circles) and strike direction (triangles) of a fracture set tilted away from the vertical by the angle θ. The background parameters are $V_{P0b} = 2$ km/s, $V_{S0b} = 1$ km/s, $\epsilon_b = 0.3$, $\delta_b = 0.2$ and $\gamma_b = 0.4$. The fracture weaknesses are (a) $\Delta_T = 0.2$, $\Delta_N = 0$ (fluid-saturated cracks) and (b) $\Delta_T = 0.2$, $\Delta_N = 0.8$ (dry cracks).

FIG. 3. Traveltime of the reflected $PS_2(\mathrm{PS}_\perp)$-wave computed in the dip direction of a fracture set. The reflector is horizontal at a depth of 1 km. The background parameters and fracture weaknesses are $V_{P0b} = 2.0$ km/s, $V_{S0b} = 0.9$ km/s, $\epsilon_b = 0.15$, $\delta_b = 0.05$, $\gamma_b = 0.05$, $\Delta_T = 0.1$, $\Delta_N = 0.4$ (corresponds to dry fractures); the fractures are tilted by $\theta = 25^\circ$ from the vertical.

FIG. 4. Pure-mode NMO ellipses in a horizontal fractured layer with the parameters given in Fig. 3. The thin outer circle corresponds to a velocity of 2 km/s.

FIG. 5. Fracture and background parameters of the model with dry fractures from Fig. 3 obtained by nonlinear inversion using the exact equations for the NMO ellipses and vertical velocities. The dots mark the correct values; the error bars correspond to the 95% confidence intervals. The confidence intervals for the parameters V_{P0b}, V_{S0b} and θ (not shown) are 2.8%, 0.5% and 3.6°, respectively.

FIG. 6. Same as Fig. 5 but for fluid-filled fractures ($\Delta_N = 0$). The 95% confidence intervals for the parameters V_{P0b}, V_{S0b} and θ (not shown) are 2.0%, 0.5% and

1.7°, respectively.

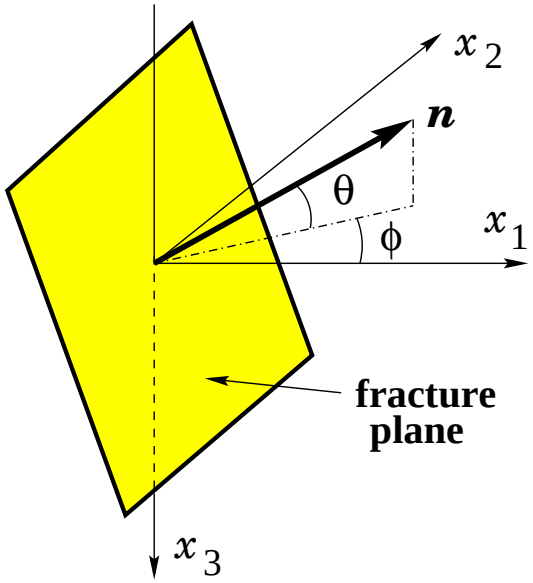

FIG. 1. Orientation of a fracture set is described by the dip θ and azimuth ϕ of the vector $\boldsymbol{n}$ orthogonal to the fracture plane. Since the background is azimuthally isotropic, we assume that the fracture strike is parallel to the x_2-axis, and $\phi = 0$.

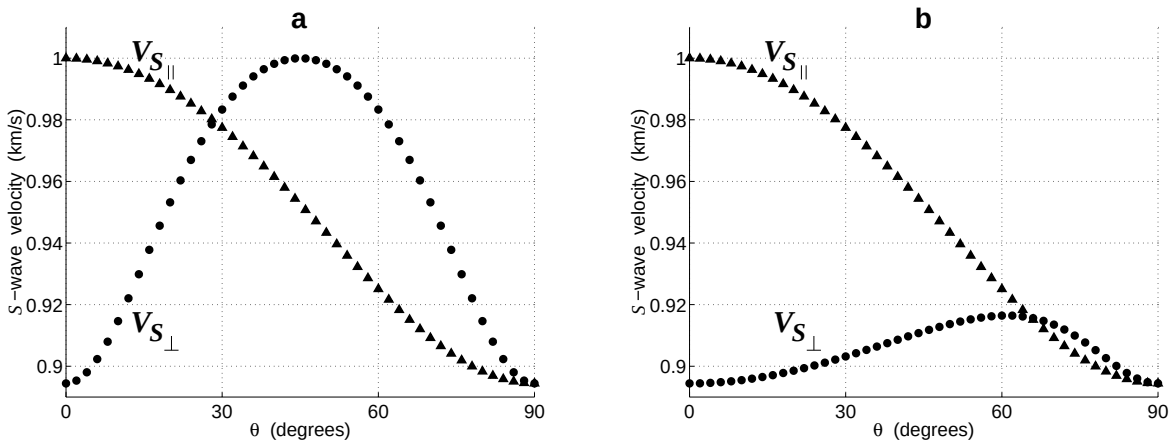

FIG. 2. Exact vertical phase velocities of the shear waves polarized in the dip plane (circles) and strike direction (triangles) of a fracture set tilted away from the vertical by the angle θ. The background parameters are $V_{P0b} = 2$ km/s, $V_{S0b} = 1$ km/s, $\epsilon_b = 0.3$, $\delta_b = 0.2$ and $\gamma_b = 0.4$. The fracture weaknesses are (a) $\Delta_T = 0.2$, $\Delta_N = 0$ (fluid-saturated cracks) and (b) $\Delta_T = 0.2$, $\Delta_N = 0.8$ (dry cracks).

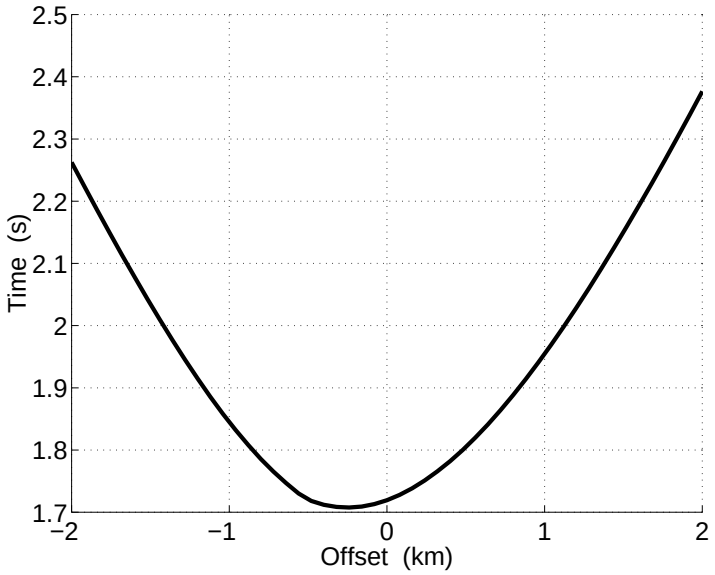

FIG. 3. Traveltime of the reflected $PS_2(\mathrm{PS}_\perp)$-wave computed in the dip direction of a fracture set. The reflector is horizontal at a depth of 1 km. The background parameters and fracture weaknesses are $V_{P0b} = 2.0$ km/s, $V_{S0b} = 0.9$ km/s, $\epsilon_b = 0.15$, $\delta_b = 0.05$, $\gamma_b = 0.05$, $\Delta_T = 0.1$, $\Delta_N = 0.4$ (corresponds to dry fractures); the fractures are tilted by $\theta = 25^\circ$ from the vertical.

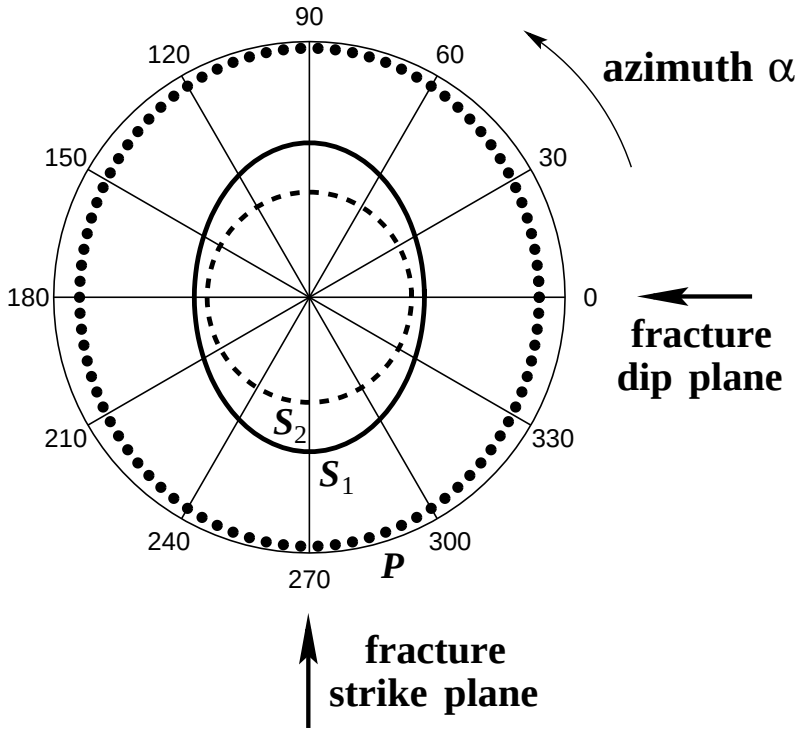

FIG. 4. Pure-mode NMO ellipses in a horizontal fractured layer with the parameters given in Fig. 3. The thin outer circle corresponds to a velocity of 2 km/s.

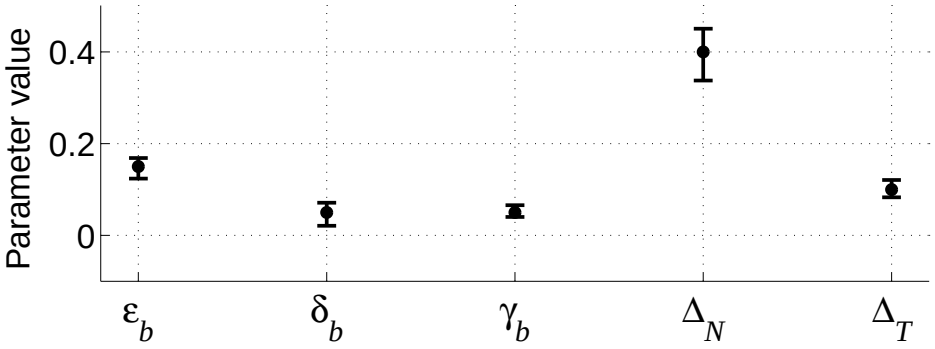

FIG. 5. Fracture and background parameters of the model with dry fractures from Fig. 3 obtained by nonlinear inversion using the exact equations for the NMO ellipses and vertical velocities. The dots mark the correct values; the error bars correspond to the 95% confidence intervals. The confidence intervals for the parameters V_{P0b}, V_{S0b} and θ (not shown) are 2.8%, 0.5% and 3.6°, respectively.

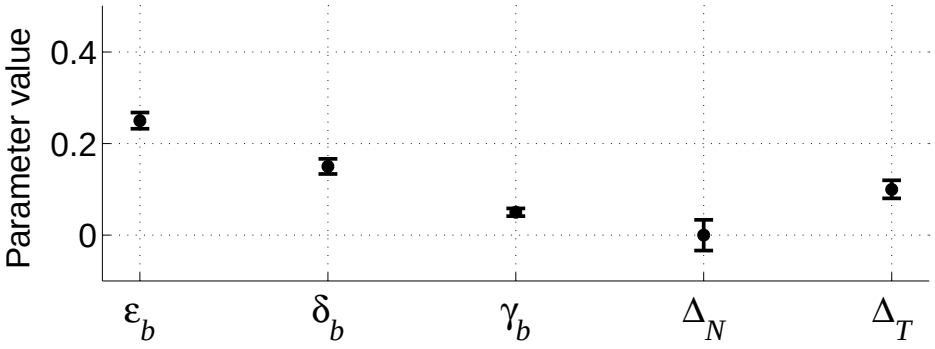

FIG. 6. Same as Fig. 5 but for fluid-filled fractures ($\Delta_N = 0$). The 95% confidence intervals for the parameters V_{P0b}, V_{S0b} and θ (not shown) are 2.0%, 0.5% and 1.7°, respectively.